A Low Power Interference Robust IR-UWB Transceiver SoC for WBAN Applications

Yuan Gao, Xin Liu, Yuanjin Zheng, Shengxi Diao, Weida Toh, Yisheng Wang, Bin Zhao, Minkyu Je and Chun-Huat Heng

Abstract An integrated 3–5 GHz impulse radio ultra-wideband (IR-UWB) transceiver system on chip (SoC) for wireless body area network (WBAN) applications is presented. To enhance system robustness against narrow band interference (NBI) signals, receiver low noise amplifier (LNA) input matching network is optimized to reject out-band NBI. A noncoherent energy detection scheme using analog squarer with band-pass filtering is utilized to increase the rejection to both in-band/out-band NBI. A low-power pulse synchronization algorithm is implemented in the digital baseband. The proposed transceiver achieves energy efficiency of 0.3 and 4.3 nJ/bit for TX and RX respectively and a receiver sensitivity of -92 dBm (BER $= 10^{-3}$) for UWB on-off keying (OOK) signal at 1 Mb/s pulse rate. The measured maximum in-band/out-band SIR for BER $= 10^{-3}$ is -33 and -47 dB, respectively.

Keywords Impulse radio ultra-wideband (IRUWB) · Wireless body area network (WBAN) · Transceiver · System on chip (SoC) · Medical monitoring

Introduction

Wireless body area network (WBAN) technology is developing rapidly in recent years as it provides a platform to support various sensors deployment around human body for emerging healthcare applications [1, 2]. Figure 1 illustrates a typical application scenario of WBAN technology in personal healthcare. Different physiological signals such as electrocardiogram (ECG), respiration rate, body temperature,

Y. Gao (✉) · X. Liu · S. Diao · W. Toh · B. Zhao · M. Je
Institute of Microelectronics, A*STAR, Singapore, Rep. of Singapore
e-mail: gaoy@ime.a-star.edu.sg

Y. Zheng · Y. Wang
School of Electrical and Electronic Engineering,
Nanyang Technological University, Singapore, Rep. of Singapore

C.-H. Heng
Department of Electrical and Computer Engineering,
National University of Singapore, Singapore, Rep. of Singapore

M. R. Yuce (ed.), *Ultra-Wideband and 60 GHz Communications for Biomedical Applications,* DOI 10.1007/978-1-4614-8896-5_2,

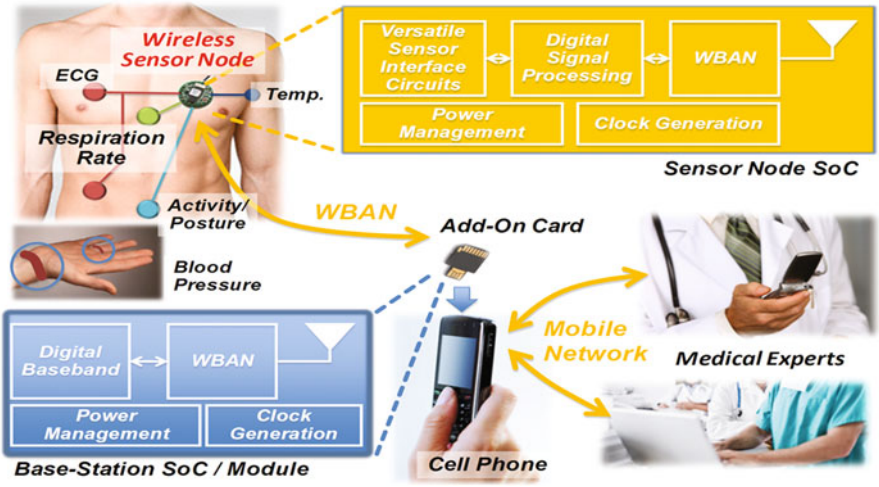

Fig. 1 Application scenario of wireless body area network (WBAN) technology in personal healthcare

etc. are acquired by individual sensors attached to the human body. The data are combined at the wireless sensor node and transmitted through the WBAN wireless link to a portable personal base-station which can be installed in a smart phone. The data can be further transferred to a remote healthcare center for detailed analysis and diagnosis by medical professionals. Benefiting from technology advances in biomedical sensor, wireless communication, and integrated circuits, the WBAN technology helps to develop miniaturized, lightweight, ultra-low power physiological healthcare surveillance and monitoring devices, for the improvement of human lives [3–5].

Among all kinds of wireless communication systems suitable for WBAN applications, impulse radio ultra-wideband (IR-UWB) is well known for its unique low-power and high data-rate merits [6]. In an IR-UWB system, information is encoded in a very narrow pulse of a few nanoseconds, which only occupies a small fraction of the symbol period. Exploiting the low duty cycle of IR-UWB signaling, the transceiver can achieve low power operation with high energy efficiency. Noncoherent energy detector (ED) can be employed in the IR-UWB receiver, which eliminates power consuming local oscillator and carrier synchronization blocks. The simplified receiver architecture also leads to power reduction and faster turn on time. Therefore, IR-UWB has been chosen by IEEE 802.15.6 task group as one of the physical layer solution for high data rate WBAN system [7].

In a noncoherent ED receiver, the energy of the received signal is measured and compared to an appropriately selected threshold to determine the presence of a signal. For an additive white Gaussian noise (AWGN) channel and completely unknown signal parameters, ED provides the optimal detection performance [8]. However, the performance of the conventional ED is sensitive to the narrowband interferences (NBI). The strong signals from other existing narrow-band wireless communication systems can saturate the high-gain IR-UWB RF front-end and ED. The major

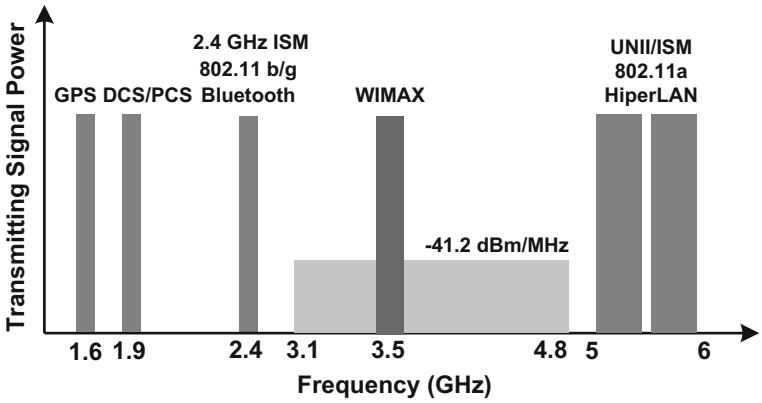

Fig. 2 Major interferers for the 3–5 GHz impulse radio ultra-wideband (IR-UWB) system

interferers to the 3–5 GHz IR-UWB system are illustrated in Fig. 2. The 2.4 GHz industrial science medical (ISM) band is currently adopted by 801.11 b/g WLAN and Bluetooth. The 5 GHz Unlicensed National Information Infrastructure (UNII)/ISM band is divided into two, 5.2–5.8 GHz sub-bands. Besides, in-band interferer such as WiMAX service occupies the 3.4–3.9 GHz bands. Effective suppression of both in-band/out-of-band interference signals is critical for the deployment of IR-UWB communication system for practical applications.

In this chapter, an interference robust single-chip IR-UWB transceiver SoC including RF transceiver and digital baseband for WBAN applications is presented. In-band/out-of-band interference suppression functions are incorporated using notch filter in low noise ampliflier (LNA) matching network and an ED with frequency conversion characteristics. A low-power pulse synchronization algorithm is implemented in the digital baseband. The proposed IR-UWB system on chip (SoC) has been successfully applied in a continuous vital signal monitoring system and the performance is verified with measurement results.

System Architecture

The block diagram of the proposed IR-UWB transceiver SoC is shown in Fig. 3 [9]. A fully differential transceiver radio frequency (RF) front-end architecture is adopted in this design to provide good suppression of common mode noise in power supply and noise through substrate coupling. It also provides direct connection to the external differential antenna, without using bulky and lossy balun circuit. Time-division multiplexing is adopted to activate the TX and RX alternately through the control of on-chip T/R switch.

On the TX side, a fast startup LC voltage-controlled oscillator (VCO) controlled by TX data, generates the UWB pulse and then is amplified by a driving amplifier (DA).

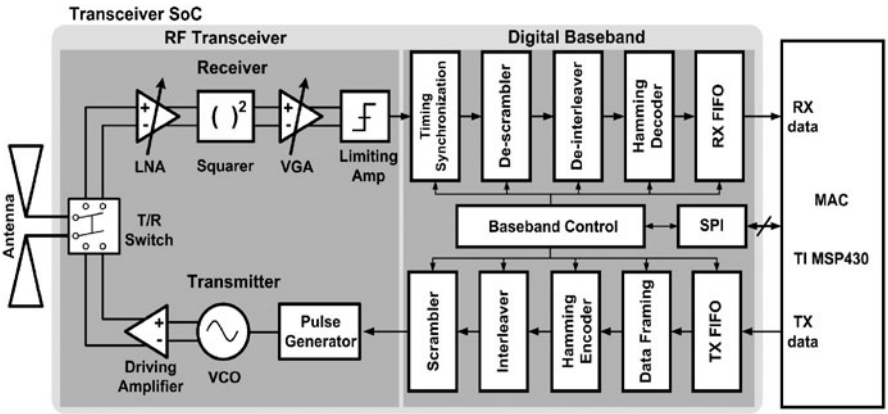

Fig. 3 Block diagram of the impulse radio ultra-wideband (IR-UWB) transceiver system on chip (SoC)

Both VCO and driving amplifier only consume power during the pulse generation. On the RX side, the weak received signal from antenna is amplified by an LNA, followed by a squarer as energy detector to recover the signals. A variable gain amplifier (VGA) further boosts the signal level and finally the analog signal is digitized by a limiting amplifier. Narrow band interference (NBI) is suppressed by embedded notch filter in LNA and the frequency conversion characteristics of energy detector.

Digital baseband (DBB) provides synchronization, forward error correction (FEC) coding/decoding, and data framing/de-framing for the TX and RX data respectively. The media access control (MAC) layer is implemented in a Texas Instrument (TI) low-power microcontroller MSP430 which communicates with transceiver SoC through SPI and dedicated data lines.

In an IR-UWB system, the transmitted signal consists of a sequence of pulses, modulated by information symbols. For the purpose of studying the mechanism of NBI suppression, we focus on the signals in a single period in the interval $(0, t_p)$, where t_p is the pulse period. To simplify the analysis, the multipath effect and circuit noise contribution are neglected. The LNA output signal is expressed as:

$$r(t) = s(t) + i(t) \quad t \in (0, t_p), \tag{1}$$

where *s(t)* is the UWB signal and *i(t)* is the NBI signal.

The carrier-based UWB pulse signal *s(t)* can be approximated as a Gaussian pulse, modulated by a carrier signal, which is expressed as:

$$s(t) = A_s e^{-\pi\left(\frac{t-t_0}{2\tau}\right)^2} \cos(2\pi f_c t), \tag{2}$$

where A_s is the amplitude of the pulse, 2τ represents the duration of the pulse, t_0 is the time delay and f_c is the carrier frequency.

The narrowband interferer is modeled as a single-tone interferer, shown in Eq. (3) for analytical simplicity. However, the results derived for a single-tone interferer also apply for an interferer which can be modeled as a band-limited random process. This will be validated by the measurement results.

$$i(t) = A_i \cos(2\pi f_i t) \tag{3}$$

Based on the input/output relationship of an ideal squarer, the squarer output $V_{out}(t)$ can be written as:

$$\begin{aligned} V_{out}(t) &= K[s(t) + i(t)]^2 = K\left[A_s e^{-\pi\left(\frac{t-t_0}{2\tau}\right)^2} \cos(2\pi f_c t) + A_i \cos(2\pi f_i t)\right]^2 \\ &= K A_s^2 e^{-2\pi\left(\frac{t-t_0}{2\tau}\right)^2} \frac{1+\cos(2\pi f_c t)}{2} + K A_i^2 \frac{1+\cos(2\pi f_i t)}{2} \\ &\quad + K A_s A_i e^{-\pi\left(\frac{t-t_0}{2\tau}\right)^2} \{\cos[2\pi (f_c - f_i) t] + \cos[2\pi (f_c + f_i) t]\} \end{aligned} \tag{4}$$

It can be observed from Eq. (4) that, after squarer operation, *s(t)* would be split into two parts. The first part is a squared Gaussian pulse, down-converted to baseband while the second part is an up-converted squared Gaussian pulse with carrier frequency of $2f_c$. Similarly for NBI *i(t)*, it will generate a DC component and a high-frequency component at $2f_i$. A band-pass filter can filter out the DC NBI signal and the high-frequency components. The low-frequency component of squarer output is used for energy detection because signal amplification in low-frequency region consumes less power and requires simpler circuit implementation. However, there is also a down-converted intermodulation component of *s(t)* and *i(t)* to $f_c - f_i$. This component may fall in the baseband pass-band and affects the receiver performance, depending on the frequency difference between the carrier and the interferer.

Key Circuit Blocks

Transmitter

Figure 4 shows the schematic of the proposed UWB transmitter. The LC VCO core consists of a cross-coupled NMOS pair (NM_{1-2}) and an on-chip LC tank (L_{1-2}, C_{1-2}) [10]. The VCO oscillation frequency can cover the frequency range of 3.5–4.5 GHz by tuning varactor control voltage V_{tune} through SPI. The pulse generator consists of a three-stage delay cell and an edge combiner to convert the standard non-return-to-zero (NRZ) baseband data to return-to-zero (RZ) pulse to control the on/off of the VCO through the tail transistor NM_3. It should be noted that NM_3 does not function exactly as a tail bias current transistor, but rather acts as a control switch to power on/off the VCO. Its sizing is chosen to ensure sufficiently fast turn on time for the pulse generation. Compared to conventional UWB pulse generator with pulse shaping filter [11], high output swing, which is critical for robust communication, can be easily

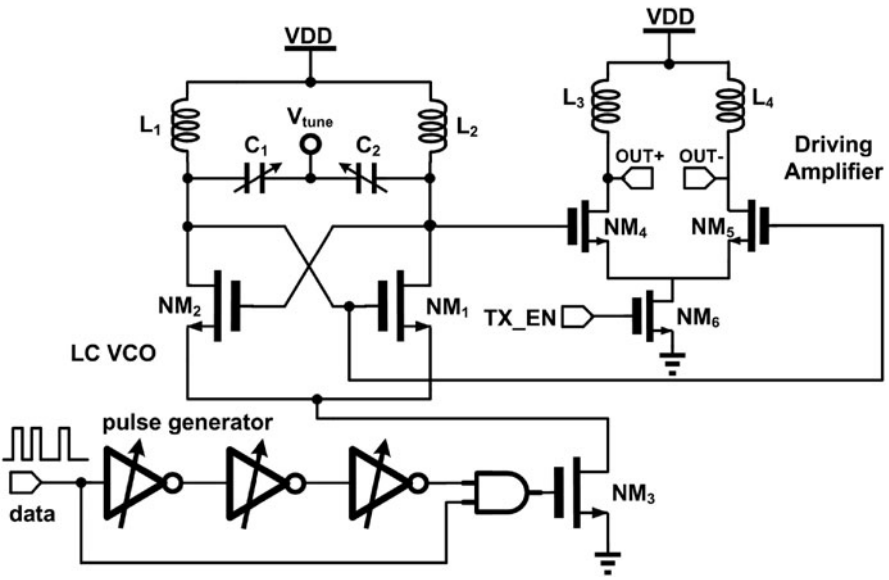

Fig. 4 Schematic of the ultra-wideband (UWB) transmitter

attained due to the positive feedback action of VCO and bandwidth boosting LC components . By turning on the LC VCO only during the pulse generation, transmitter with high energy efficiency can be designed and constant power efficiency can be maintained across a wide range of data rate. Differential DA consists of NM_{4-5} and L_{3-4}, they can further boost the output swing and also isolate the VCO core from the external loading to reduce VCO pulling effect. NM_6 acts as a switch to enable/disable DA, it is controlled by the TX enable signal (TX_EN) from digital baseband.

Low Noise Amplifier

A four-stage fully differential variable gain LNA is designed for the RX front-end. Figure 5 shows the schematic of first two stages. Current reuse topology is utilized to stack the two-stage cascaded amplifiers into one current-reuse cell. Hence, the power consumption is reduced by half while the power gain is maintained. Same architecture is used for the third and fourth stages without the input matching network. Similar current reuse technique has been applied in single-ended LNA [12], however at least four inductors are required in one current-reuse cell, excluding the input matching circuit. Hence, a four-stage differential LNA will require eight inductors in total, occupying a very large area. In this design, the symmetry of the differential LNA is exploited and the single-ended inductors are replaced with differential inductors to save chip area.

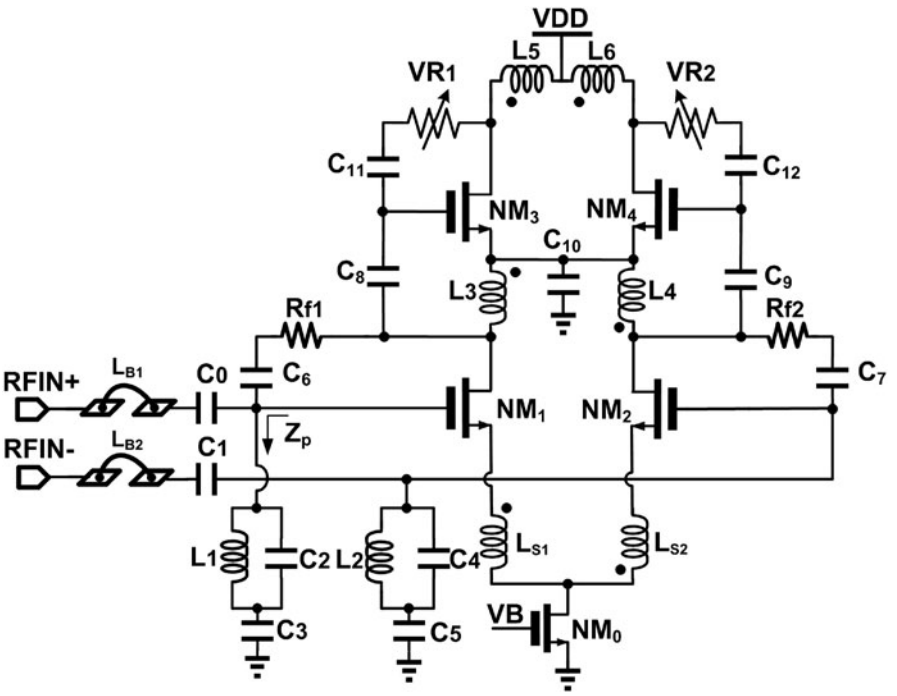

Fig. 5 Schematic of the fully differential low noise amplifier (first and second stages)

A modified LC ladder network input matching network is used for wideband matching. It should be noted that L_{B1} and L_{B2} are implemented with bonding wires, L_1 and L_2 are off-chip high-Q inductors. In addition, the DC decoupling capacitor is optimized to control the transmission zero position to enhance the out-band interference rejection around 2.4 GHz. The shunt LC resonant tank input impedance Z_p can be expressed as:

$$Z_p = \frac{1 - \omega^2 L_1(C_2 + C_3)}{(1 - \omega^2 L_1 C_2) \cdot j\omega C_3} \tag{5}$$

The transmission zero can be calculated as:

$$\omega_p = \frac{1}{\sqrt{L_1(C_2 + C_3)}} \tag{6}$$

By optimizing the value of L_1 and C_2, C_3, the transmission zero can be used to attenuate out-of-band interference at 2.4 GHz while maintaining input matching in 3–5 GHz band. As illustrated in Fig. 6, when C_2 increases from 2 to 4 pF, the notch frequency decreases from 2.48 to 1.9 GHz.

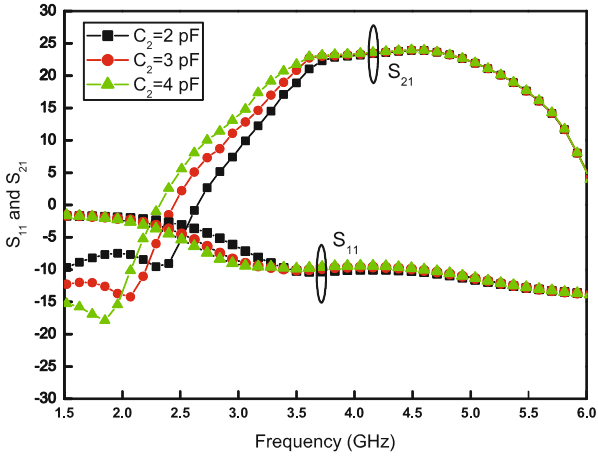

Fig. 6 Simulation results of low noise amplifier (LNA) S_{11} and S_{21} versus C_2 variation

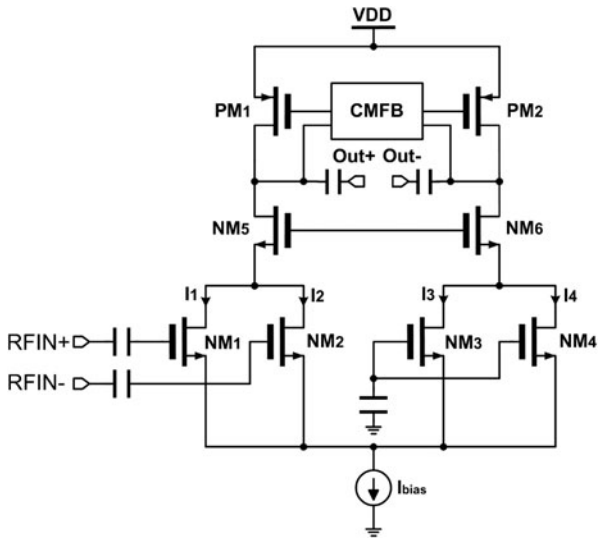

Fig. 7 Schematic of the squarer

Squarer

The schematic of the proposed squarer is shown in Fig. 7 [13]. Transistors NM_{1-4} have the same sizing and the same DC biasing point in saturation region. Differential RF input signals are fed into NM_{1-2} to perform squaring function while NM_{3-4} are AC grounded, so as to cancel the output DC components. The total biasing current is set by the current source I_{bias}. NM_{5-6} are cascode stages to enhance the squarer output impedance. Large output impedance is desired to boost the output voltage swing, hence active load is used here using PMOS transistors PM_{1-2} and they are biased with a common-mode feedback (CMFB) circuit. It is well known that active load value decreases with increasing frequency due to the large parasitic capacitance.

However, since the target signal is in the low frequency range, we can take advantage of this characteristic to implement the embedded band-pass filter function. Ignoring the channel length modulation and transistor body effect, the drain current of NM_{1-4} can be given as:

$$I_1 = \frac{\beta}{2}\frac{W}{L}\left(V_B + \frac{V_{in}}{2} - V_{th}\right)^2 \tag{7}$$

$$I_2 = \frac{\beta}{2}\frac{W}{L}\left(V_B - \frac{V_{in}}{2} - V_{th}\right)^2 \tag{8}$$

$$I_3 = I_4 = \frac{\beta}{2}\frac{W}{L}(V_B - V_{th})^2 \tag{9}$$

The squarer output voltage can be expressed as:

$$V_{out} = I_{out} \cdot R_{load} = (I_1 + I_2 - I_3 - I_4) \cdot R_{load} = \frac{\beta}{4}\frac{W}{L}v_{in}^2 R_{load} \tag{10}$$

where ß is the transistor constant, R_{load} represents the equivalent total loading resistance at the output of the squarer. From (Eq. 10), it can be observed that, besides using larger transistors for the transconductance stage, increasing the squarer load resistance is another efficient way to boost the squarer output voltage. At low frequency, R_{load} is limited by the squarer output resistance, since the squarer output is connected to the gate of next stage which has very high input impedance. The output resistance of proposed squarer can be expressed as:

$$R_{load} \approx r_{o,PM1} || \left[\left(1 + \frac{g_{m,NM5} \cdot r_{o,NM1}}{2}\right) \cdot r_{o,NM5}\right] \tag{11}$$

where r_o is the transistor output resistance and g_m is the transistor transconductance. The large R_{load} together with the parasitic capacitance and the input capacitance of the next stage will form a band-pass filter to suppress the low-frequency and high-frequency NBI components after the squaring operation. The optimized R_{load} should be the one that maximizes the squarer output voltage without significantly filtering the down-converted Gaussian envelope component by the squarer .

Analog Baseband

The block diagram of VGA and comparator is shown in Fig. 8. The VGA consists of a three-stage fixed gain (12 dB) and a variable gain stage (− 15–15 dB). Coarse gain tuning is achieved by selecting the number of fixed gain stages to use. Fine gain tuning is varied by controlling the current ratio in the variable gain stage to achieve resolution of 1 dB/step. The output of the VGA is then connected to a limiting amplifier which output full-swing pulse to the digital baseband. In order to ensure

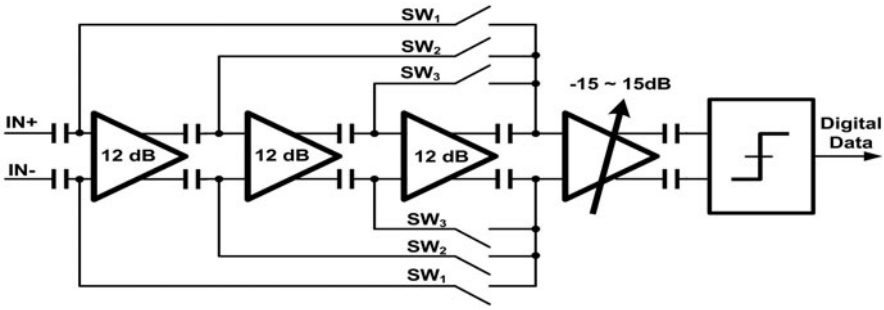

Fig. 8 Schematic of the analog baseband

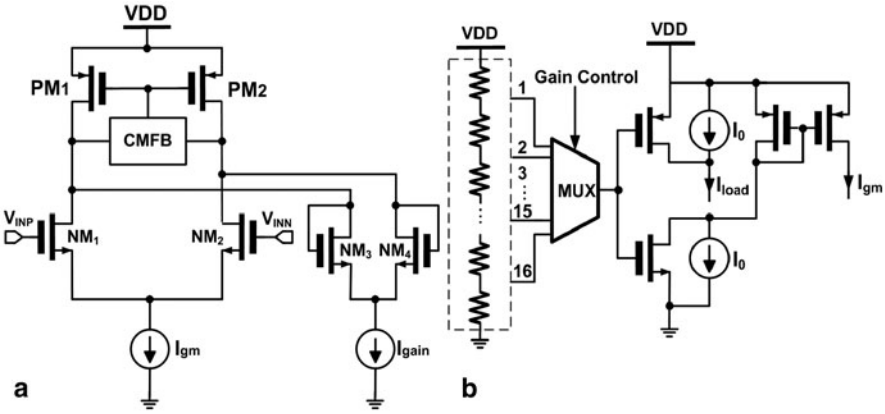

Fig. 9 Schematic of the **a** g_m-cell and **b** fine gain control circuit

accurate gain control, closed-loop amplifiers are typically used [14, 15]. However, a closed-loop amplifier consumes a large amount of current. An alternative way to achieve accurate gain control is to use the g_m-ratioed amplifier as shown in Fig. 9a at low current consumption [16]. The amplifier gain can be approximately expressed as $g_{m,in}/g_{m,load}$, where $g_{m,in} = g_{m1-2}$ and $g_{m,load} = g_{m3-4}$. By proper setting of the size for transistor M_1–M_4, and the current of I_{gm} and I_{load}, the amplifier gain can be accurately controlled.

More importantly, the ratios of transistor size and current deviate very little from the design values in CMOS implementation by proper circuit design and layout techniques. Both the fixed gain and the fine tuning amplifiers are implemented with the g_m-ratioed architecture with different sizes. For the fine tuning amplifier, the accurate gain step is realized by controlling the current ratio of I_{gm} and I_{load} in a logarithmic way. The current steering circuit is depicted in Fig. 9b. The gain control signal is generated using a resistor voltage divider. One of the 16 control references is selected by a MUX, controlled by gain control word from SPI. By a proper selection of transistor M_{7-8} sizes and current I_0, a logarithmic amplifier can be realized based on the g_m-ratioed amplifier [16].

http://www.springer.com/978-1-4614-8895-8

Ultra-Wideband and 60 GHz Communications for Biomedical Applications

Yuce, M.R. (Ed.)

2014, XI, 261 p. 195 illus., 52 illus. in color., Hardcover
ISBN: 978-1-4614-8895-8